MODELING OF THE NONLINEAR DYNAMIC BEHAVIOR OF A MICRO-AERIAL-VEHICLE (MAV) IN AN ENVIRONMENT OF A TURBULENT ATMOSPHERE

T.Kordes, M.Buschmann, P.Vörsmann
Institute of Aerospace Systems (Institut für Luft- und Raumfahrtsysteme)
Technical University of Braunschweig
Hermann-Blenk-Str. 23, D-38108 Braunschweig, Germany

Abstract

This paper describes the nonlinear modeling of the six degrees of freedom motion of a Micro Aerial Vehicle (MAV) in a turbulent atmosphere, and presents the results.

The Institute of Aerospace Systems of the Technical University of Braunschweig (Germany) is currently developing a Micro Aerial Vehicle (MAV). The goal of this research project named "CAROLO" is the manufacturing of a completely autonomous microplane with a wingspan of approximately 40 cm.

For this purpose, a set of nonlinear differential equations has been derived that takes the highly nonlinear dynamic behavior and special MAV-related effects into account. The resulting simulation tool is a basis for a later design of the flight control system (FCS), and the development of navigation filters using GPS and INS.

Nomenclature

Φ, Θ, Ψ	Eulerian angles
γ, χ	angle of climb, heading
p, q, r	components of $\underline{\Omega}$
u, v, w	components of $\underline{V}$
x, y, z	position
m	mass
g	acceleration due to gravity
S	wing area
b	span
c	reference chord
$\underline{V}$	velocity
W, Q, A	drag, side force, lift
α, β	angle of attack, sideslip
η, κ, ξ	rudder deflections
i_F	engine installation angle
F	thrust
$\omega_x, \omega_y, \omega_z$	rotational speed of the propulsion system
I_x, I_y, I_z	moments of inertia
$\underline{D}$	angular momentum
$\underline{\Omega}$	rotational aircraft speed
T	time constant
T_t	dead time
K	gain
C_{mq}, C_{lp}, C_{nr}	damping derivatives
Λ	aspect ratio
$\bar{q}$	dynamic pressure
r	lever arm

Subscripts

$(\ )_a$	wind axes
$(\ )_f$	body axes
$(\ )_g$	earth fixed
$(\ )_H$	elevator
$(\ )_s$	rudder

1 Introduction

1.1 Introduction

The term Micro Air Vehicle describes a class of aircraft whose size is of the order of magnitude of small birds. Visions for the future are the development of aircraft as small as insects. They represent not only the smallest man-made aircraft, but also miniaturized, intelligent, and autonomous flying robots. Due to their special characteristics, there is a wide range of application for these tiny vehicles. Equipped

with special sensors, they can fulfill reconnaissance and surveillance missions like air quality or traffic monitoring. They are able to monitor hostage situations or locate sources of contamination after chemical or radioactive accidents.

1.2 The Project "CAROLO"

Several approaches were made worldwide towards the development of a microplane with sub-meter wingspan. For example, [1] and [2] describe remote-controlled microplanes with wingspans less than 15 cm. However, the integration of a completely autonomous navigation capability is still a big challenge. At the Institute of Aerospace Systems, the project "CAROLO" does not try to minimize size and weight of the microplane, but puts emphasis on the capability of fully autonomous navigation. The name "CAROLO" is derived from the name of the "Technical University Carolo Wilhelmina of Braunschweig". Figure 1 shows the first microplane prototype "CAROLO I".

Figure 1: Prototype "CAROLO 1"

The propulsion system is designed in pusher configuration. The first approach provides two control surfaces, an elevator at the front unit and an aileron implemented in the wing. Some of the design parameters are listed below:

span b	0.40 m
mass m	360 g
design speed V_C	18 m/s
duration of flight T	40 min
range R	45 km

Figure 2 shows a transparent view of "CAROLO 1" with all subsystems.
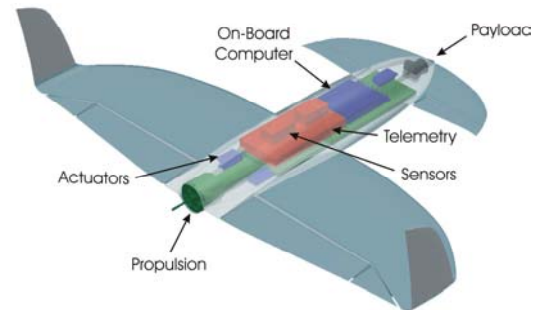
Figure 2: Anatomy of "CAROLO 1"

2 System Dynamics

Due to their small mass and moments of inertia, these vehicles show highly dynamic characteristics, especially in a real environment with a turbulent atmosphere. The usual assumption of small angles, particularly the Euler angles, is not valid. Hence the state space formulation with the linearized equations of motion is not sufficient to describe the coupled dynamics of these vehicles. Because of the fact that the vehicle and the wind velocity have the same order of magnitude, the simplification of linear aerodynamics may also not be applied. There are also some special MAV related effects like the angular momentum of the propulsion system which have to be considered. In addition, it is necessary to describe the actuator dynamics to obtain a description of the overall system behavior.

The atmosphere's movement is the major cause of the disturbance of the trajectory and flight attitude. Especially these small vehicles are very sensitive to these real world influences. For this reason static and turbulent wind models are implemented in the simulation environment.

In order to take these effects into account, a model with the complete nonlinear differential equations of motion and nonlinear aerodynamics is derived. This model provides a basis for a later design of the flight control system (FCS) and the development of navigation filters using GPS and INS.

The following subchapters describe the theoretical background.

2.1 Database

As mentioned above it is not sufficient for a microplane to apply linear aerodynamics. Due to their relatively slow cruise speed large aerodynamic angles such as angle of attack α and sideslip β may appear. To get the aerodynamic forces and moments over the full flight envelope, wind tunnel readings have been taken at the Institute of Fluid Mechanics at the Technical University of Braunschweig. The aerodynamic loads have been determined as a function of angle of attack α, sideslip β, elevator deflection η, aileron deflection ξ and flap deflection κ. The following ranges have been investigated:

$$-10° < \alpha < 40°$$
$$-32° < \beta < 32°$$
$$-15° < \eta < 15°$$
$$-15° < \xi < 15°$$
$$-8° \ < \kappa < 12°$$

The result is a 5-dimensional parameter field for the dimensionless force coefficients C_X, C_Y, C_Z and the dimensionless moment coefficients C_L, C_M, C_N.

Figure 3 shows "CAROLO 1" during its first wind tunnel flight.

Figure 3: Wind tunnel tests

The dimensionless damping moments C_{mq}, C_{lp} and C_{nr} as a consequence of the aircraft's rotational speed can be calculated approximately with some simplifications. The corresponding equations can be found in [3] and [4].

It is:

Roll Damping Derivative

$$C_{lp} = \frac{\partial C_l}{\partial\left(\frac{p \cdot b}{2 \cdot V}\right)} = -\frac{1}{4} \cdot \frac{\pi \cdot \Lambda}{\sqrt{\frac{\Lambda^2}{4} + 4} + 2} \tag{1}$$

Yaw Damping Derivative

$$C_{nr} = \frac{\partial C_n}{\partial\left(\frac{r \cdot b}{2 \cdot V}\right)} = C_{YS\beta S} \cdot \frac{V}{\overline{V}_S} \cdot V_S \cdot \frac{2 \cdot r_S}{b} \tag{2}$$

with

$$C_{YS\beta S} = \frac{2\pi \cdot \Lambda}{\sqrt{\Lambda_S^2 + 4} + 2} \tag{3}$$

Pitch Damping Derivative

$$C_{mq} = \frac{\partial C_m}{\partial\left(\frac{q \cdot c}{V}\right)} = -C_{AH\alpha H} \cdot \sqrt{\frac{\overline{q}_H}{\overline{q}}} \cdot \frac{S_H}{S} \cdot \left(\frac{r_H}{c}\right)^2 \tag{4}$$

Figure 4 shows the lift curve for different elevator deflections with flaps in neutral position. Flow separation begins at approximately $\alpha = 15°$. "CAROLO 1" shows very uncritical stall behavior.
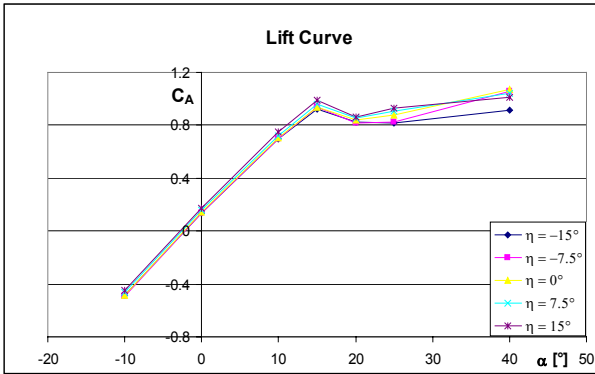
Figure 4: Lift vs. angle of attack

Figure 5 illustrates the corresponding lift vs. drag curve without rudder deflection. The point of an optimal lift to drag ratio is marked. This point determines the design speed of $V_C = 18$ m/s.
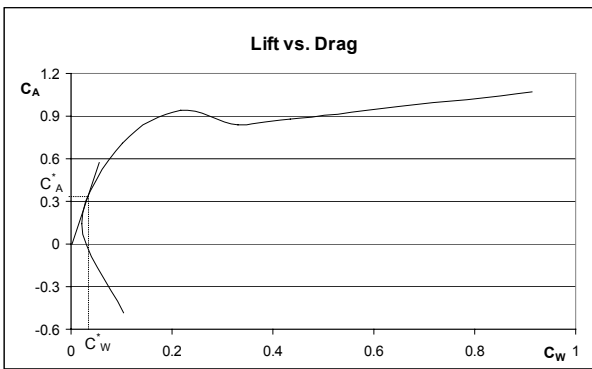
Figure 5: Lift vs. Drag

2.2 Forces and Moments

Aerodynamics

In order to get dimensionless aerodynamic forces and moments C_i the following reference values are used:

- dynamic pressure $\quad \bar{q} = \dfrac{\rho}{2} V_A^2$

- wing area $\qquad$ S
- span $\qquad$ b
- reference chord $\quad$ c

The coefficients are denoted in body fixed axes. The vector of the aerodynamic forces can be written as:

$$\underline{F}_f{}^A = \begin{bmatrix} X^A \\ Y^A \\ Z^A \end{bmatrix}_f = \underline{\underline{M}}_{fa} \cdot \begin{bmatrix} -W \\ Q \\ -A \end{bmatrix}_a =$$

$$= \underline{\underline{M}}_{fa} \frac{\rho}{2} V_A{}^2 S \begin{bmatrix} -c_W(\alpha, q_A, \eta) \\ c_Q(\beta, p_A, r_A, \xi, \zeta) \\ -c_A(\alpha, q_A, \eta) \end{bmatrix}_a \qquad (5)$$

The matrix $\underline{\underline{M}}_{fa}$ describes the transformation from wind into body axes and is defined as follows:

$$\underline{\underline{M}}_{fa} = \begin{bmatrix} \cos\alpha\cos\beta & -\cos\alpha\sin\beta & -\sin\alpha \\ \sin\beta & \cos\beta & 0 \\ \sin\alpha\cos\beta & -\sin\alpha\sin\beta & \cos\alpha \end{bmatrix} \qquad (6)$$

The corresponding moments are:

$$\underline{Q}_f{}^A = \begin{bmatrix} L^A \\ M^A \\ N^A \end{bmatrix}_f = \frac{\rho}{2} V_A{}^2 S \begin{bmatrix} \dfrac{b}{2} c_L(\beta, p_A, \xi) \\ c \cdot c_M(\alpha, q_A, \eta, \kappa) \\ \dfrac{b}{2} c_N(\beta, r_A, \xi) \end{bmatrix}_f \qquad (7)$$

Propulsion System

The vectors of thrust forces and moments can be written directly in body fixed axes. Neglecting the interaction of aerodynamics and propeller stream the resulting terms are:

$$\underline{F}_f{}^F = \begin{bmatrix} \cos i_F \\ 0 \\ -\sin i_F \end{bmatrix} \cdot F \qquad (8)$$

$$\underline{Q}_f^F = \begin{bmatrix} x_F \\ y_F \\ z_F \end{bmatrix} \times \begin{bmatrix} \cos i_F \\ 0 \\ -\sin i_F \end{bmatrix} F = \begin{bmatrix} -y_F \sin i_F \\ z_F \cos i_F + x_F \sin i_F \\ -y_F \cos i_F \end{bmatrix} F \quad (9)$$

Due to the small system mass and the microplane's high thrust to mass ratio the influence of propulsion torque has to be considered.

$$\underline{Q}_f^T = \begin{bmatrix} \dfrac{P}{\omega} \\ 0 \\ 0 \end{bmatrix} = \begin{bmatrix} \dfrac{F \cdot V_A}{\omega} \\ 0 \\ 0 \end{bmatrix} = \begin{bmatrix} \dfrac{F \cdot V_A}{2\pi \cdot f} \\ 0 \\ 0 \end{bmatrix} \quad (10)$$

Additionally, the propulsion system has even more influence on the dynamic system behavior. The reason is the fact that a part of the propulsion system rotates in body fixed axes but the whole system itself rotates regarding the earth fixed system. In order to investigate the gyroscopic effect the following equations have been derived [5]:

$$\underline{Q}_f^M = \frac{d\underline{D}}{dt} = \frac{d\underline{D}}{dt} + \underline{\Omega} \times \underline{D} \quad (11)$$
$$= \underline{\underline{I}}_{\text{Prop}} \cdot \underline{\dot{\omega}} + \underline{\Omega} \times \underline{\underline{I}}_{\text{Prop}} \cdot \underline{\omega}$$

The single components are:

$$\underline{Q}_f^M = \begin{bmatrix} I_{x,\text{Prop}} \cdot \dot{\omega}_x \\ I_{y,\text{Prop}} \cdot \dot{\omega}_y \\ I_{z,\text{Prop}} \cdot \dot{\omega}_z \end{bmatrix} + \begin{bmatrix} q \cdot I_{z,\text{Prop}} \cdot \omega_z - r \cdot I_{y,\text{Prop}} \cdot \omega_y \\ r \cdot I_{x,\text{Prop}} \cdot \omega_x - p \cdot I_{z,\text{Prop}} \cdot \omega_z \\ p \cdot I_{y,\text{Prop}} \cdot \omega_y - q \cdot I_{x,\text{Prop}} \cdot \omega_x \end{bmatrix} \quad (12)$$

The propeller is just rotating about the body fixed x axes. That means:

$$\omega_y = \omega_z = 0$$

On the assumption that the rotary speed is constant follows:

$$\dot{\omega}_x = \dot{\omega}_y = \dot{\omega}_z = 0$$

This leads to a simple equation for the gyroscopic moment [6] and must be treated like an inertia term.

$$\underline{Q}_f^M = \begin{bmatrix} 0 \\ r \cdot I_{x,\text{Prop}} \cdot \omega_x \\ -q \cdot I_{x,\text{Prop}} \cdot \omega_x \end{bmatrix} \quad (13)$$

Mass forces

The vector of the mass force can be written in an earth fixed system as follows:

$$\underline{G}_g = \begin{bmatrix} 0 \\ 0 \\ 1 \end{bmatrix} \cdot m \cdot g \quad (14)$$

With the transformation from the earth fixed into the body fixed coordinate system this term can be expressed as:

$$\underline{G}_f = \begin{bmatrix} -\sin\Theta \\ \cos\Theta \cdot \sin\phi \\ \cos\Theta \cdot \cos\phi \end{bmatrix} \cdot m \cdot g \quad (15)$$

2.3 Differential Equations

The derivation of the set of the nonlinear differential equations is based on the following simplifying assumptions:

1. The earth is considered as a non-rotating reference system. This assumption effects no errors in subsonic and transonic flight.

2. The aircraft is a rigid body. Additional elastic degrees of freedom are neglected. Due to the small moments of inertia in conjunction with the stiff construction this simplification is valid.

3. The aerodynamic loads at the tail and the fuselage are assumed to be quasi-stationary. Therefore, transient effects are neglected.

Generally, the 6 degrees of freedom motion of a rigid aircraft can be described by a set of 4 nonlinear vector differential equations.
The first and the second are developed from the classical works of Newton.

Translation

$$m\left(\frac{dV_K}{dt}\right)^g_n = m\left[\left(\frac{dV_K}{dt}\right)^n_n + \underline{\Omega}^{gn}_n \times \underline{V}_{Kn}\right] = \sum F \tag{17}$$

Rotation

$$\underline{\underline{T}}_n\left(\frac{d\underline{\Omega}^{gn}_n}{dt}\right)^g_n = \left[\underline{\underline{T}}_n\left(\frac{d\underline{\Omega}^{gn}_n}{dt}\right)^n_n + \underline{\Omega}^{gn}_n \times \underline{\underline{T}}_n\underline{\Omega}^{gn}_n\right] = \sum M \tag{18}$$

The 3rd vector differential equation describes the relation between the aircraft's attitude (Eulerian angles) and the body fixed rotational speed.

$$\begin{bmatrix}\dot{\Phi}\\\dot{\Theta}\\\dot{\Psi}\end{bmatrix} = \begin{bmatrix}1 & \sin\Phi\cdot\tan\Theta & \cos\Phi\cdot\tan\Theta\\0 & \cos\Phi & -\sin\Theta\\0 & \dfrac{\sin\Phi}{\cos\Theta} & \dfrac{\cos\Phi}{\cos\Theta}\end{bmatrix}\cdot\begin{bmatrix}p_K\\q_K\\r_K\end{bmatrix}_f \tag{19}$$

The last differential equation supplies the aircraft's position by integrating the velocity.

$$\frac{d\underline{s}_g}{dt} = \underline{V}_{Kg} = \begin{bmatrix}\dot{x}\\\dot{y}\\\dot{z}\end{bmatrix}_g = \begin{bmatrix}\Delta N\\\Delta E\\-\dot{H}\end{bmatrix} = \begin{bmatrix}\cos\gamma\cos\chi\\\cos\gamma\sin\chi\\-\sin\gamma\end{bmatrix}V_K \tag{20}$$
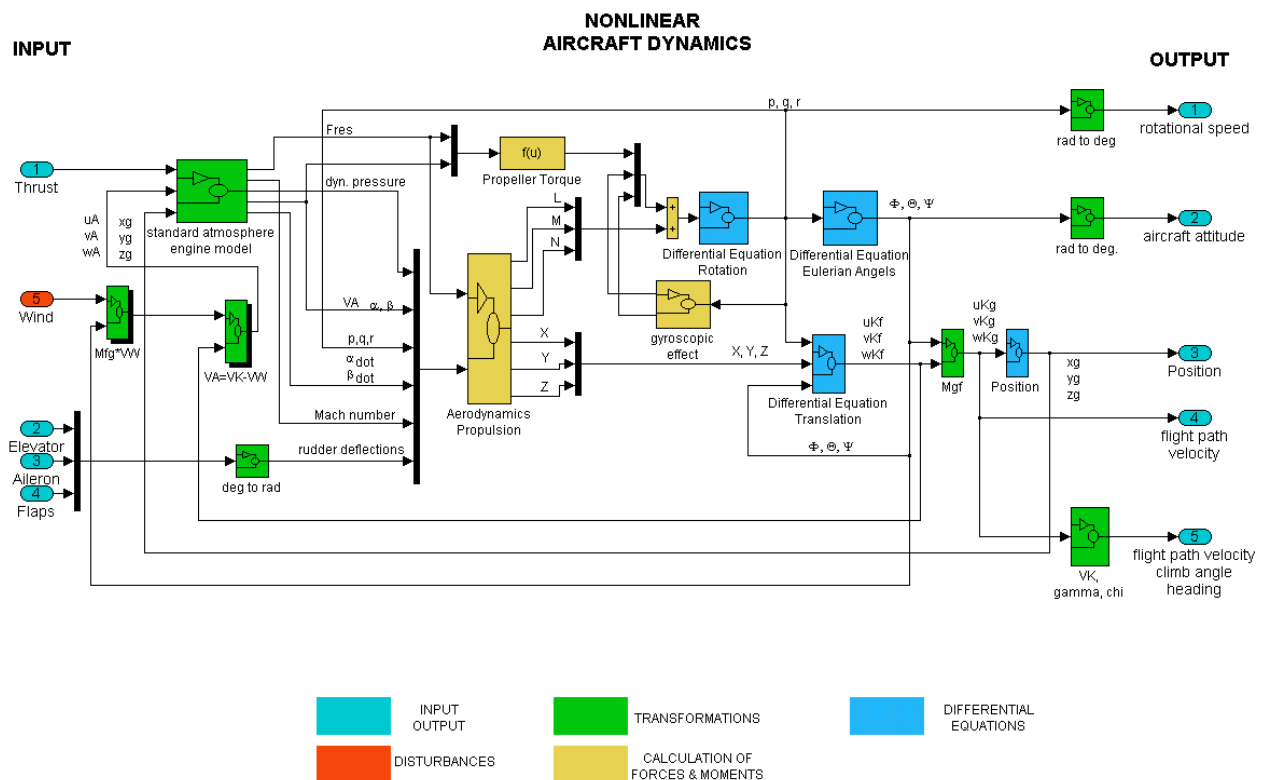
Figure 6: Block diagram of aircraft dynamics

Figure 6 shows the block diagram of the aircraft dynamics. For better clarity just the upper level is shown. This diagram contains all equations from subchapter 2.1 up to and including subchapter 2.3.

2.4 Actuator Dynamics

Due to its small mass and moments of inertia a Micro-Aerial-Vehicle is a very dynamic system. The high angular rates require fast actuators to control the aircraft. To get a realistic description of the overall system dynamics it is necessary to model the actuator dynamics as well. For this reason the transfer behavior of the planned actuator system has been acquired. Figure 7 shows the investigated servo drive.

The light servo has a mass of 3 grams and consists of a small electric motor, a gearbox, and a control logic.
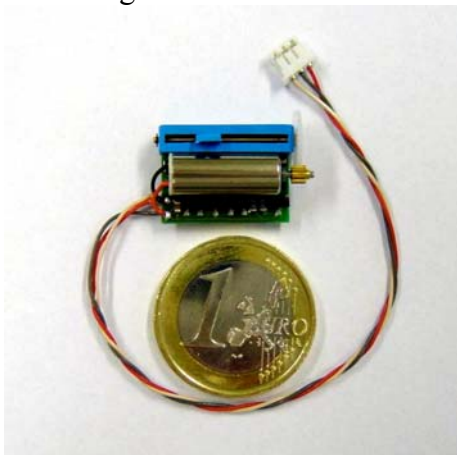
Figure 7: WES-Technik Light Servo 3.0

To get a mathematical model of the actuator dynamics some tests have been carried out. A defined control input has been compared with the measured system output. It was shown that the mechanical system has first order transfer behavior. In addition a dead time exists, mainly caused by the control logic.

In the time domain the actuator dynamics can be written as [7]:

$$y_S(t) = u(t - T_t) \cdot K \cdot \left(1 - e^{-\frac{t}{T}} \right) \qquad (21)$$

The corresponding term in the frequency domain is:

$$y_S(s) = \frac{K}{Ts + 1} \cdot e^{-j\omega T_t} \cdot u(s) \qquad (22)$$

The constants K, T_t and the time constant T have been determined.
Figure 8 shows a comparison between the commanded input, the measured output, and the modeled output.
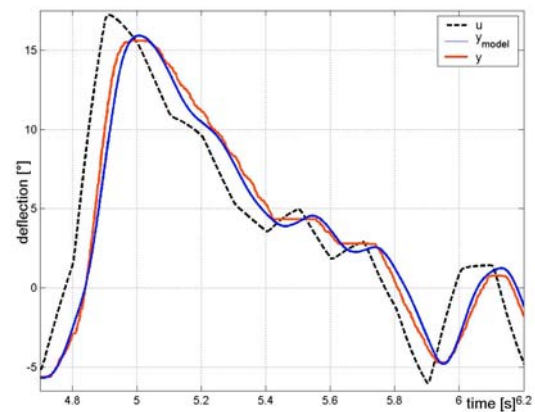
Figure 8: Servo in- and output, model output

Figure 8 shows that the theoretical model of the servo dynamics matches the real behavior sufficiently.

2.5 Modeling of Wind

The developed simulation tool provides the opportunity to investigate the influence of wind on the aircraft's dynamic behavior. The following options are implemented:

1. stationary wind
2. Dryden model of atmospheric turbulence
3. measured wind data

Due to its simplicity the Dryden model was chosen to simulate the atmospheric turbulence. In [3] a simple method is shown to prepare the Dryden model for simulation purposes. Figure 9 illustrates the procedure.

Figure 9: Simulation of turbulence

The filter equations are:

$$F_{uw}(j\omega) = \sqrt{2\sigma_u^2 T_u} \cdot \frac{1}{1 + j\omega T_u}$$

$$F_{vw}(j\omega) = \sqrt{\sigma_v^2 T_v} \cdot \frac{1 + j\omega\sqrt{3}T_v}{(1 + j\omega T_v)^2} = F_{ww}(j\omega)$$

(23)

2.6 Simulation Tool
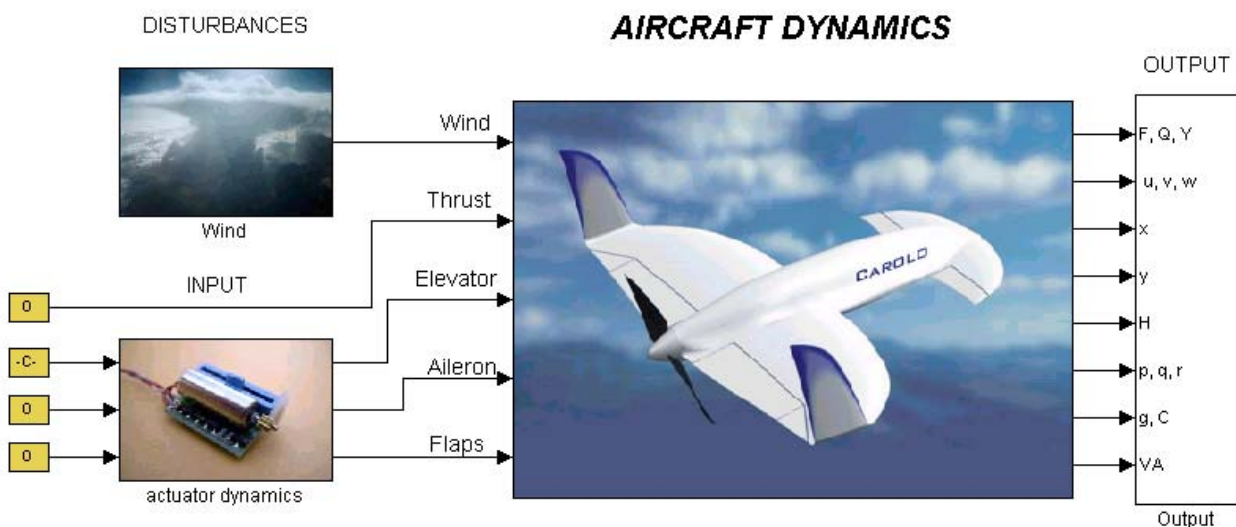
Figure 10: Simulation Tool

3   Results

This chapter presents some example results of the microplane's dynamic behavior. First of all the gyroscopic effect is shown.

Gyroscopic effect

Figures 11 to 13 show the Eulerian angles due to an elevator deflection of $\Delta\eta = 2°$ for one second. The resulting rotational speed q about the pitch axes causes a changing of the yaw angle as expected with equation (13). Due to the increasing rotation about the yaw axes the bank angle is affected as well. This effect is mainly
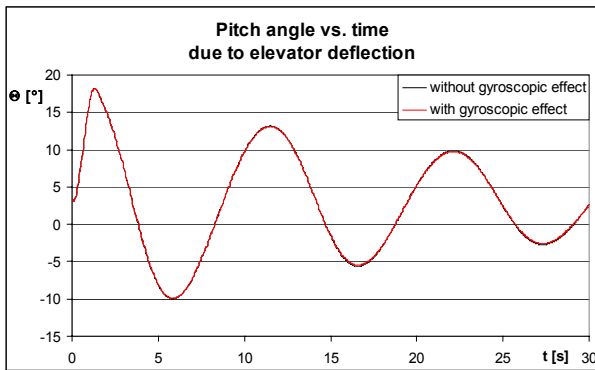
Figure 11: Pitch angle vs. time

caused by the aerodynamic coupling of the roll moment due to a yaw motion. A negative yaw motion causes a negative roll motion due to the higher lift at the right wing.
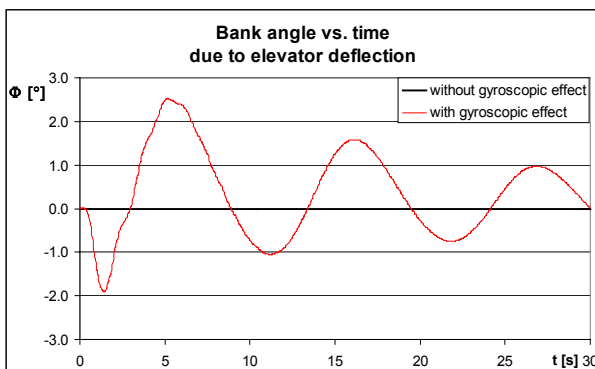
Figure 12: Bank angle vs.time

All figures reflects the phugoid mode of the aircraft. It can be seen that the oscillation is weakly damped with a time period of about 10 seconds.

The results show that the gyroscopic effect has a clear influence on the aircraft's dynamic behavior. It results in a coupling of the microplane's longitudinal and lateral motion.
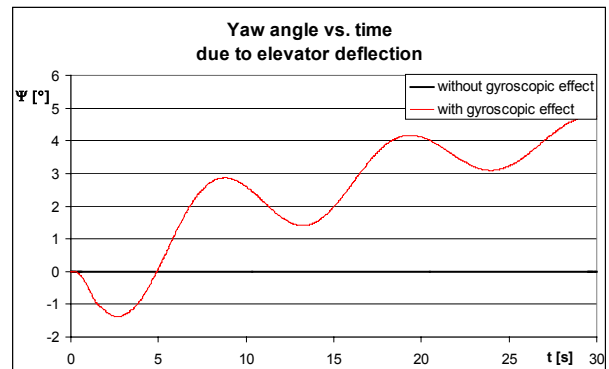
Figure 13: Yaw angle vs. time

Wind sensitivity

The next three figures show the aircraft's response to the influence of turbulent wind. To simulate the wind the Dryden model was used with maximum wind velocities of about 7m/s.

The time plots contain three different cases, a flight without damper, a flight with pitch and yaw damper and a flight with damping system in consideration of the actuator dynamics.
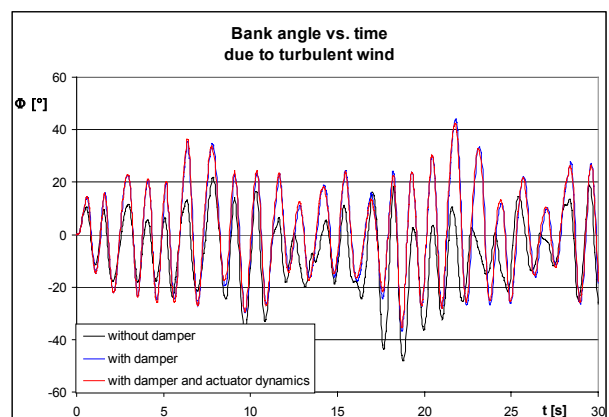
Figure 14: Bank angle vs. time

The yaw damper was realized by using the ailerons to stabilize the yaw motion. This

explains the higher bank angles with damping system compared to the case without damper in figure 14. The corresponding plot of the pitch and yaw angle is much smoother with the activated damping system. Against that the actuator dynamics has just a small influence on the aircraft's motion. This influence is mainly caused by the time delay of the servo drives.
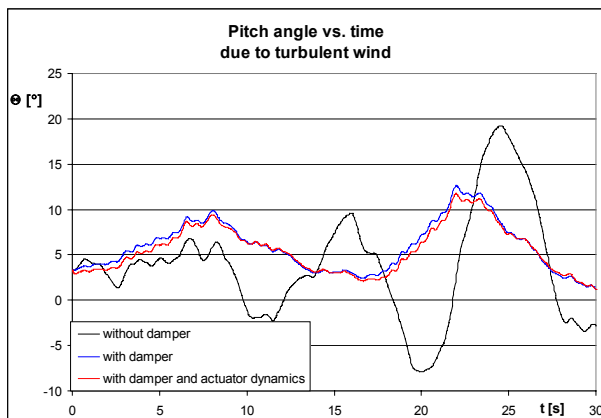
Figure 15: Pitch angle vs. time
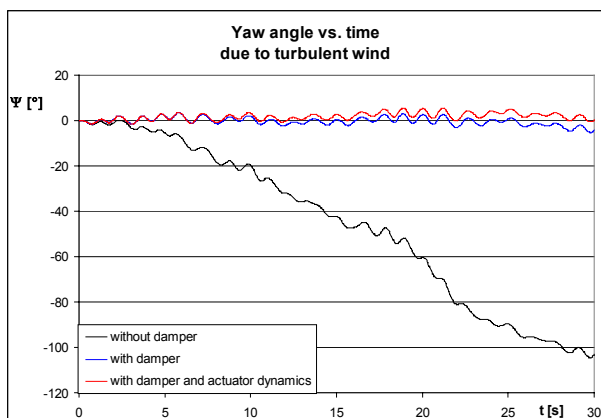
Figure 16: Yaw angle vs. time

However, these plots underline the aircraft's sensitivity to these real world influences, especially without a stabilizing damping system.

4 Summary and Outlook

This paper described the nonlinear modeling of a microplane's dynamic behavior including the actuator system. It was shown that it is necessary to consider the gyroscopic effect of the rotating propulsion system. Normally, this effect is neglected for conventional aircraft

where the overall sytem mass is much larger than the engine mass. Additionally, there is a need to describe the nonlinear aerodynamics at the high angle of attack region. This results from the comparatively low cruise speed. Under real world conditions the wind speed can be of the same order of magnitude that results in high angles of attack and sideslip.

The developed simulation tool provides a basis for an advanced description of a microplane's dynamic behavior. It will be used for a later flight control system design as a first step towards autonomous navigation. Moreover, this simulation environment will be used to investigate the effect of sensor errors and will help to develop navigation filters for an integrated navigation system using GPS and INS.

References

[1] Grasmeyer J.M, Keennon M.T**.** Development of the Black Widow Micro Air Vehicle. *39th AIAA Aerospace Sciences, Meeting&Exhibit*, Jan. 2001, Reno, NV, AIAA 2001-0127

[2] Morris S. J. Design and flight test results for micro sized fixed wing and VTOL aircraft. *Proceedings of 1st International Conference on Emerging Technologies for Micro Air Vehicles*, Georgia Institute of Technology, Atlanta, Georgia, 19-20 Feb. 1997

[3] Brockhaus, R. *Flugregelung*. Springer Verlag 2002, ISBN 3-540-41890-3

[4] Schlichting, Tuckenbrodt. *Aerodynamik des Flugzeuges*. Springer Verlag 1960

[5] Szabó I. *Höhere Technische Mechanik*. 6th edition, Springer Verlag, 2001, ISBN 3-540-67653-8

[6] Etkin B, Reid L.D. *Dynamics of Flight*. 3rd edition, John Wiley & Sons, INC, 1996

[7] Merz L, Jaschek H. *Grundkurs der Regelungstechnik*. 11th edition, Oldenbourg Verlag, 1992